Improved model-based infrared reflectometry for measuring deep trench structures

Chuanwei Zhang,[1] Shiyuan Liu,[2,*] Tielin Shi,[1] and Zirong Tang[1]

[1]*Wuhan National Laboratory for Optoelectronics, Huazhong University of Science and Technology, Wuhan, Hubei 430074, China*

[2]*State Key Laboratory of Digital Manufacturing Equipment and Technology, Huazhong University of Science and Technology, Wuhan, Hubei 430074, China*

**Corresponding author: shyliu@mail.hust.edu.cn*

Received July 1, 2009; accepted September 8, 2009;
posted September 16, 2009 (Doc. ID 113682); published October 13, 2009

Model-based infrared reflectometry (MBIR) has been introduced recently for characterization of high-aspect-ratio deep trench structures in microelectronics. The success of this technique relies heavily on accurate modeling of trench structures and fast extraction of trench parameters. In this paper, we propose a modeling method named corrected effective medium approximation (CEMA) for accurate and fast reflectivity calculation of deep trench structures. We also develop a method combining an artificial neural network (ANN) and a Levenberg–Marquardt (LM) algorithm for robust and fast extraction of geometric parameters from the measured reflectance spectrum. The simulation and experimental work conducted on typical deep trench structures has verified the proposed methods and demonstrated that the improved MBIR metrology achieves highly accurate measurement results as well as fast computation speed. © 2009 Optical Society of America

OCIS codes: 120.0120, 300.6340, 050.6624, 050.2065.

1. INTRODUCTION

Deep trench structures with high aspect ratio have been widely used in microelectronics such as capacitors in advanced dynamic random access memory (DRAM) devices that adopt bottle trench structures with a very high aspect ratio, i.e., of more than 50:1 [1,2]. As deep trench devices have been packed more tightly, the critical dimension (CD) and depth dependent features must now be monitored to ensure process control. Many conventional methods, such as scanning electron microscopy (SEM) and atomic force microscopy (AFM), have been applied for the occasional, periodic, or quasi-continuous monitoring of the features mentioned above. Although SEM is a traditional technique for measuring trench profile [3], it does not satisfy the requirements of high-volume manufacturing and on-line monitoring because of the disadvantage of low throughput and destruction of sample. AFM is a nondestructive method [4], but it is capable of measuring only shallow trenches with low aspect ratio because of the limitations of AFM tips. Several optical metrology techniques have also been advanced to meet the need for process control in the semiconductor industry. Scatterometry is one of the well-known optical techniques that has gained considerable interest in the industrial environment for trench metrology [5,6]. It relies on measuring diffraction efficiency from periodic trench patterns such as photoresist gratings, and it is typically operated within the wavelength range from ultraviolet (UV) to visible light with a trend toward deeper UV in order to keep pace with the shrinking dimensions of the structures [5]. Scatterometry requires rigorous coupled wave analysis (RCWA) modeling with extremely high computational intensity, and it has been mainly applied to measure mask patterns with shallow trench structures [6]. Model-based infrared reflectometry (MBIR) is another optical metrology that has been introduced recently for measuring high-aspect-ratio periodic trench structures [7–9]. The trench structure is modeled as a multilayer thin film stack with effective medium approximation (EMA) theory, and the reflectance spectrum is measured in the midinfrared wavelength range, from which the trench parameters are extracted by solving an inverse spectral problem. Compared with SEM and AFM, the MBIR technique is a noncontact and nondestructive metrology for deep trench structures [7].

The success of MBIR metrology relies heavily on accurate forward modeling and fast calculation of the infrared metrology process, which still remains as one challenge. RCWA theory is commonly used for modeling in scatterometry, and it can achieve optical responses with very high accuracy; however, the calculation is quite time-consuming. EMA theory is an attractive modeling tool as it allows for a complex trench structure to be modeled as a film stack with each layer having an effective optical property [7]. After modeling with EMA, the simulated reflectance spectrum of the trench structure can be rapidly calculated using the Fresnel equation. This EMA based MBIR metrology has been successfully applied in the measurement of deep trenches in DRAMs and other power devices [8,9]. However, the zeroth-order EMA adopted in MBIR for modeling of one-dimensional (1-D) arrays of rectangular deep trenches can achieve acceptable accuracy only in the static-limit region with wavelengths much larger than the trench pitch [7]. As in the short wavelength range, zeroth-order EMA needs to be improved to increase the modeling accuracy. The zeroth-

 © 2009 Optical Society of America

order EMA of S polarization has also been applied to two dimensional (2-D) arrays of trenches such as square lattices of cylindrical trenches, which has been shown to result in rougher approximation of modeling than the 1-D trench arrays. In this paper, we propose a fast algorithm for reflectivity calculation of high-aspect-ratio deep trench structures by an improved modeling method named corrected effective medium approximation (CEMA) that is based on EMA, but has a dispersion-corrected term added to calculate the refractive index of each effective medium. The CEMA method is demonstrated to be not only fast in calculation but also accurate enough in comparison with the RCWA for both 1-D and 2-D trench arrays.

Another challenge in MBIR metrology is the robust and fast extraction of trench parameters from the measured infrared reflectance spectrum, which is a typical inverse spectral problem of finding an optimized set of trench parameters that results in a best match between the measured spectrum and the simulated one. Traditionally, there are mainly two approaches to solve this ill-posed inverse problem [10], namely, the library search method and the nonlinear regression method. Employing a library of scatter signature or spectra, the library search method has been commonly used to solve the inverse problem similarly encountered in scatterometry. The library is produced in advance by evaluating the forward model on a grid which covers the expected range of variation in the parameters. At run time, the measured signature is compared to each signature in the library and the measurement output is the set of parameters used to generate the signature with the best fit to the measurement. The library search method has been applied in specular scatterometry to extract CDs of integrated circuits with pseudoperiodic structures [11], and has also been employed in MBIR metrology to extract geometric parameters of trenches in power devices [9]. However, the library method has huge resource costs in computation and storage space, as the evaluation grid needs to be dense enough to produce measurement output with enough resolution. Nonlinear regression methods such as local optimization algorithms are widely used for grating metrology and design [12,13]. The iteration process with a local optimization algorithm can be finished in several iterations, but it depends heavily on the initialization. It is well understood that the optimization is nonconvex, and the iterative methods can easily lead to a local rather than a global solution. Therefore, a good initialization scheme is essential. Use of an artificial neural network (ANN) is another nonlinear regression method that is widely used in functional approximation and pattern classification applications because of its capability of modeling complex and highly non-linear functions [14]. Recently, the ANN has been adopted to simulate the relationship between the spectral reflection and grating profile in scatterometry and ellipsometry, having the possibility and potential to solve the inverse grating problem [15,16]. However, the accuracy and robustness of solving inverse problems with ANN rely much on the structure design and the network training of ANN. In this paper, we develop a method combining ANN and the local optimized Levenberg–Marquardt (LM) algorithm for fast extraction of geometric parameters from the measured reflectance spectrum, in which an initial estimate of the parameters is generated from the measured reflectance spectrum by ANN, and then the accurate result is obtained by the LM algorithm.

The remainder of this paper is organized as follows. Section 2 introduces the CEMA method for modeling of both 1-D and 2-D periodic trench structures, and then describes the ANN and LM combined method for trench parameter extraction. Section 3 provides some simulation results to show the accuracy of the CEMA-based modeling method and the robustness of the combined extraction method. Section 4 presents the experimental results to demonstrate the high accuracy and fast computation ability of the improved MBIR metrology. Finally, we draw some conclusions in Section 5.

2. METHODS

A. Modeling of Deep Trench Structures with CEMA

Deep trench structures corresponding to the advanced technology node in microelectronics are typically characterized by a pitch well into the submicrometer range and thus much smaller than the optical wavelength in the midinfrared. At wavelengths greater than the pitch of the trench structure, the infrared light propagates through the trench structure as if it were a homogeneous medium. Therefore, the deep trench structure can be represented as a layered system with a combination of homogeneous layers on the silicon substrate, and the modeling of a complex deep trench structure can be simplified to the modeling of a multilayer thin film stack. The effective refractive index can be determined from the geometry of the trench structure with the EMA approach [17]. In order to increase the modeling accuracy in MBIR metrology, we have developed a CEMA based modeling method for one-dimensional (1-D) and two-dimensional (2-D) trench structures.

First, we consider the simple structure with a 1-D array of rectangular trenches and its effective optical model as shown in Fig. 1. In the case of this 1-D subwavelength periodic trench structure, the effective permittivity is expressed as a closed-form equation of the propagation constant in the stratified medium for each polarization state [18]. In the MBIR metrology, the zeroth-order EMA adopted for modeling the 1-D trench arrays could achieve acceptable accuracy only in the static-limit regime, i.e., when the wavelength is much larger than the trench pitch, roughly at least 20 times [7]. Therefore, we propose the CEMA to increase the modeling accuracy in the short wavelength range. The CEMA adds a correction term to the zeroth-order EMA equation as

$$\varepsilon_{\mathrm{eff}} = \varepsilon_0 + B\left(\frac{1}{\lambda}\right)^2 \quad \text{(for TE and TM polarization)}, \quad (1)$$

where $\varepsilon_{\mathrm{eff}}$ represents the corrected approximation of the effective permittivity; ε_0 represents the zeroth-order approximation of the effective permittivity, which is valid only in the limit that the wavelength is much larger than the trench pitch; λ represents the wavelength of the incident light in free space; and B represents the correction

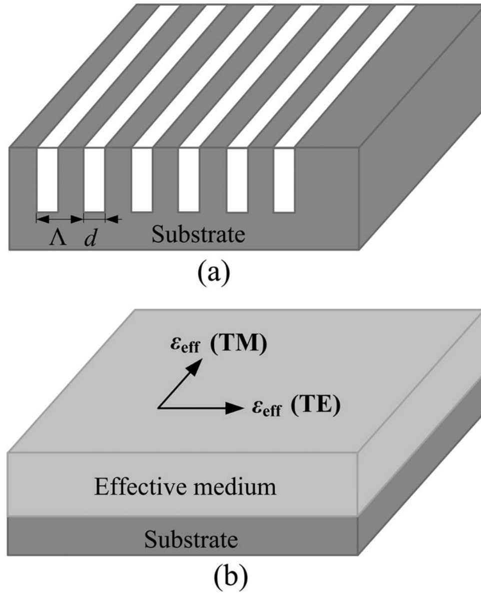

Fig. 1. Schematic drawings of (a) simple 1-D periodic trench structure and (b) its effective optical model.

factor that can be determined experimentally or analytically.

In our previous work we have determined the correction factor B experimentally [19]. Noting the transcendental dispersion equations [18], here we propose an analytical solution to the correction factor B in the TE and TM polarization states:

$$B=\frac{\pi^2}{3}f^2(1-f)^2(\varepsilon_1-\varepsilon_2)^2\Lambda^2 \quad \text{(for TE polarization)}, \tag{2}$$

$$B=\frac{\pi^2}{3}f^2(1-f)^2\left(\frac{1}{\varepsilon_1}-\frac{1}{\varepsilon_2}\right)^2\varepsilon_{\text{eff,TM0}}{}^3\varepsilon_{\text{eff,TE0}}\Lambda^2 \quad \text{(for TM polarization)}, \tag{3}$$

where $f=(\Lambda\text{-}d)/\Lambda$ represents the fill factor; d and Λ represent the trench width and the trench pitch, respectively; ε_1 and ε_2 represent the permittivity of the trench material and the filled material, respectively; and $\varepsilon_{\text{eff,TE0}}$ and $\varepsilon_{\text{eff,TM0}}$ represent the zeroth-order approximation of the effective permittivity for TE and TM polarization, respectively.

For the 2-D periodic subwavelength trench structure such as the trench array shown in Fig. 2(a), it is not so easy to determine the effective refractive index accurately as for the 1-D trench structure. The zeroth-order EMA has also been applied to the 2-D trench arrays in the MBIR metrology, but the modeling accuracy is much lower than that of the 1-D trench arrays [7]. Although many intuitive methods have been introduced to improve the modeling accuracy in the static-limit regime for the 2-D trench arrays [20,21], only rough estimates of the effective refractive indices could be obtained. Lalanne and Lalanne proposed a precise method for determining the zeroth- and second-order effective refractive indices based on Fourier decomposition of the wave propagating along

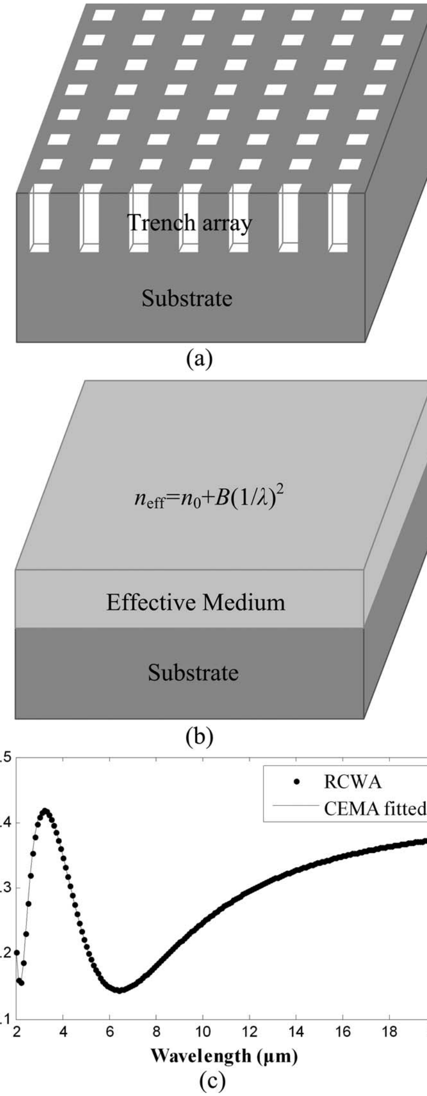

Fig. 2. (a) Simple 2-D trench structure, (b) its effective optical model, and (c) the reflectance spectrum calculated by RCWA theory and its fitted curve by CEMA method.

the direction perpendicular to the periodic structure [22]. However, this method is too computationally expensive to extract the parameters with a nonlinear regression method in MBIR metrology. Inspired by the simple form of the CEMA equation for the 1-D periodic structure, we propose a similar CEMA approach for the 2-D trench array:

$$n_{\text{eff}}=n_0+B\left(\frac{1}{\lambda}\right)^2, \tag{4}$$

where n_{eff} represents the effective refractive index for the 2-D trench array; n_0 represents the zeroth-order effective refractive index; and B represents the correction factor.

Unlike the 1-D trench structure, there is no simple analytical solution to the zeroth-order effective refractive index n_0 and the correction factor B for the 2-D trench structure. Noting that n_{eff} is independent of the depth of the trench structure with a certain substrate and filled material in the trench structure [23], we therefore propose a fitting-based method to determine n_0 and B by

finding an effective optical model of a periodic deep trench structure with effective refractive index, as shown in Fig. 2. We obtain n_0 and B by simulating the trench structure with RCWA theory and subsequently fitting the result to the reflectance curve of the effective optical model as shown in Fig. 2(b). The reflectance curve calculated by RCWA theory and the best fitted curve calculated by the CEMA method are depicted in Fig. 2(c).

With some certain values of the fill factor f between 0.2 to 0.8, the zeroth-order refractive index n_0 and the correction factor B can be calculated with the fitting-based method, as shown in Fig. 3 and Fig. 4, respectively. As an attempt to find the relationship between n_0 and f and the relationship between B and f, here we adopt the fourth-order polynomial to fit the discrete data of n_0 and B:

$$n_0 = a_0 + a_1 f + a_2 f^2 + a_3 f^3 + a_4 f^4, \tag{5}$$

$$B = b_0 + b_1 f + b_2 f^2 + b_3 f^3 + b_4 f^4, \tag{6}$$

where a_i and b_i are the polynomial coefficients to be determined by the least-squares method.

B. Parameter Extraction with ANN and LM Combined Algorithm

Because of the highly nonlinear relationship between the geometry parameters and the reflectivity of the trench structure, the extraction of the trench parameters is a typically ill-posed inverse problem. The first step toward solving this inverse problem is to define an accurate forward model, which has been mathematically described in Subsection 2.A. Figure 5 shows the forward modeling and the inverse spectral problem in MBIR metrology. Here we propose a method combining ANN and the LM algorithm to solve this inverse problem. With the initial value estimated by the ANN, the LM algorithm solves the inverse problem in an iterative fitting scheme, in which the model parameters are adjusted until the simulated reflectance spectrum fits the measured data. The optimization problem is formulated as follows:

$$\hat{P} = \arg\min_{P} \sum_{j=1}^{N} [R_{\mathrm{m}}(\lambda_j) - T\{P\}]^2$$
$$= \arg\min_{P} \sum_{j=1}^{N} [R_{\mathrm{m}}(\lambda_j) - R_{\mathrm{c}}(\lambda_j)]^2, \tag{7}$$

where $\hat{P}$ represents the optimized vector of geometric parameters; $P=[d_1,d_2,\ldots,d_K,h_1,h_2,\ldots,h_K]$ represents the vector containing geometric parameters of the deep trench structure; d_k and h_k $(k=1,2,\ldots K)$ represent the trench width and trench depth of the kth effective layer, respectively; K is the total number of the effective layers; $R_{\mathrm{m}}(\lambda_j)$ and $R_{\mathrm{c}}(\lambda_j)$ represent the measured reflectivity and theoretical simulated reflectivity, respectively; λ_j represents the jth utilized wavelength; N represents the total number of the utilized wavelengths; and $T\{\cdot\}$ represents the forward modeling function transforming the geometric parameter vector P into the theoretical simulated reflectivity $R_{\mathrm{c}}(\lambda_j)$.

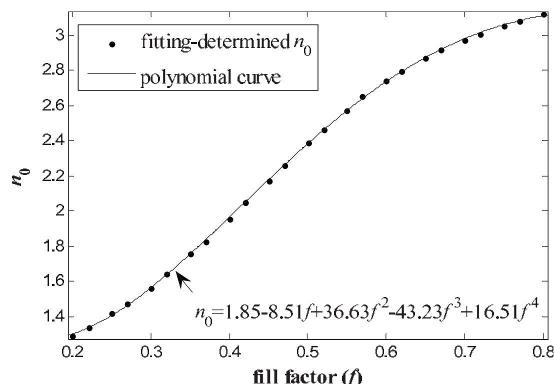

Fig. 3. Plot of fitting-determined zeroth-order refractive index by the fourth-order polynomial.

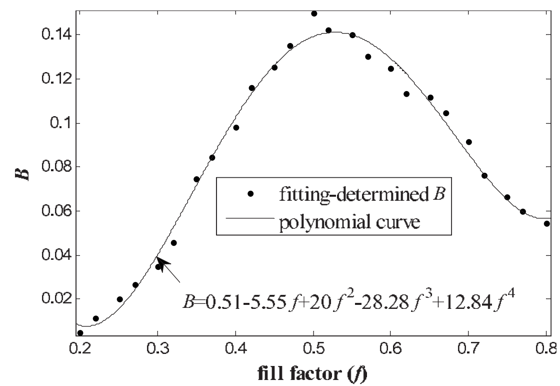

Fig. 4. Plot of fitting-determined correction factor by the fourth-order polynomial.

Figure 6 depicts the flowchart of parameter extraction with the ANN and LM combined algorithm. The extraction process is described in detail as follows.

First, an ANN of multilayer perceptron (MLP) type [14] is constructed that consists of three layers. The input and the output of the ANN are the reflectivity R and the parameter vector P, respectively. The number of neurons in the input layer and the output layer are determined by the length of the vectors R and P, respectively, and the number of neurons in the hidden layer is determined by experience. Once the structure of the ANN is decided, the mapping property of the ANN is determined by the connection weights linking the neurons of each layer.

The ANN is then trained by the back-propagation learning algorithm, which is classified as a supervised learning algorithm [14]. We use the forward CEMA mod-

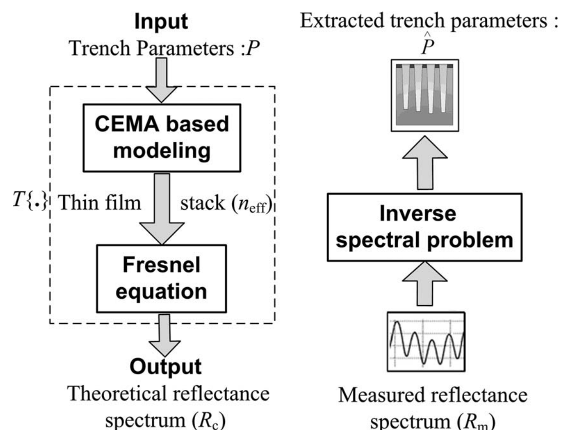

Fig. 5. Forward modeling and inverse spectral problem in MBIR metrology.

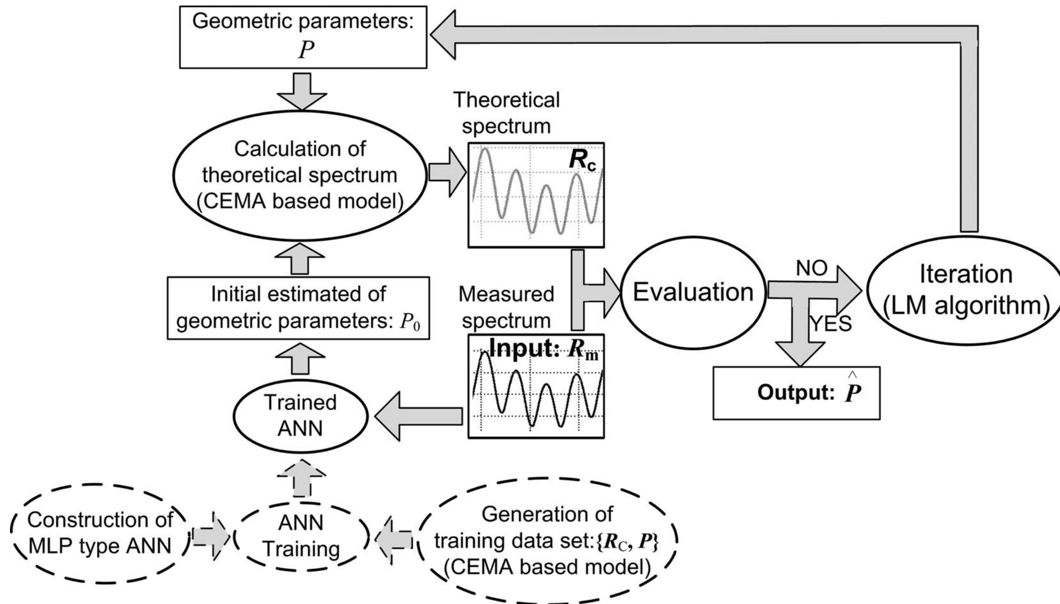

Fig. 6. Flowchart of parameter extraction using the ANN/LM combined method.

eling method in Fig. 5 to generate a training data set $\{R_c, P\}_i$, $(i=1,2,\ldots,M)$, where R_c represents the reflectance spectrum simulated from the parameter vector P, and M represents the total number of the training data set. After several hours of training the connection weights of the ANN are fixed, and the ANN that maps the reflectance spectrum to the geometric parameter vector is ready to provide an initial value for the LM iteration with an acceptable accuracy.

Finally, during MBIR metrology the raw data of the measured reflectance spectrum R_m is processed by the trained ANN, which provides an output of the geometric parameter vector P with a few percent of error. This output of ANN is then set as the initial estimate of the LM algorithm, which performs only a few iterations and further refines the estimate to an accurate final solution.

3. SIMULATIONS

A. Simulation of the CEMA Modeling Method

To demonstrate the accuracy of the proposed CEMA modeling method, we first performed simulations on the 1-D deep trench structure shown in Fig. 1(a). The 1-D structure etched on the silicon substrate composes an array of rectangular trenches with trench depth of 3 μm, trench pitch of 200 nm, and trench width of 100 nm. The simulated reflectance spectra were calculated by the RCWA theory, the zeroth-order EMA method, and the CEMA method, respectively. Figure 7 shows the simulation results in the wavenumber range of 500 to 5000 cm^{-1} in TE polarization with an incidence angle of 45°. It is observed that the CEMA method provides more accurate approximation than the zeroth-order EMA as compared with the RCWA theory in the short wavelength range, i.e., the region close to the diffraction threshold.

To further study the accuracy of the proposed CEMA modeling method, we then carried out simulations on the 2-D structure shown in Fig. 1(b), which composes an array of trench holes with trench depth of 1.5 μm, trench pitch of 200 nm, and trench width of 100 nm. The simulated reflectance spectra of the 2-D structure were calculated by the RCWA theory, the zeroth-order EMA method, and the CEMA method, respectively. Figures 8 and 9 depict the simulation results at the incidence angle of 45° in TE polarization and TM polarization states, respectively. It is clear that within the full wavenumber range of 500 to 5000 cm^{-1} the CEMA method achieves more accurate approximation than the zeroth-order EMA in comparison with the RCWA theory.

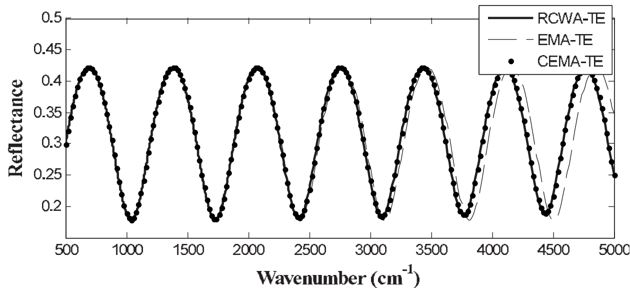

Fig. 7. Simulated reflectance spectra modeled with RCWA, zeroth-order EMA, and CEMA in TE polarization of the 1-D trench structure.

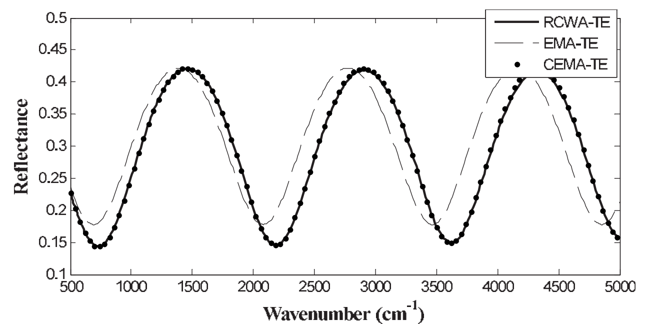

Fig. 8. Simulated reflectance spectra modeled with RCWA, zeroth-order EMA, and CEMA in TE polarization of the 2-D trench structure. The trench parameters for the simulation: trench depth 1.5 μm, trench pitch 0.2 μm, and fill factor 0.5.

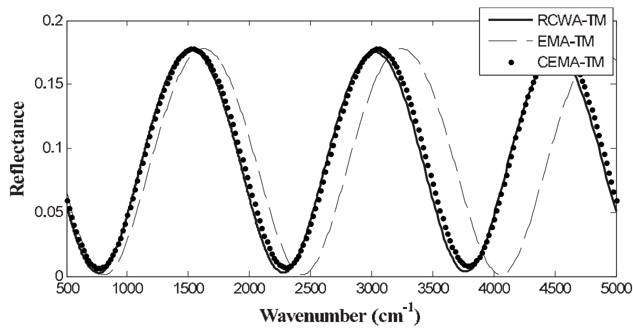

Fig. 9. Simulated reflectance spectra modeled with RCWA, zeroth-order EMA, and CEMA in TM polarization of the 2-D trench structure. The trench parameters for the simulation are as in Fig. 8.

Moreover, it was noted that the CEMA-based calculation of the reflectance spectrum could be finished in $\approx$ 100 ms on a 2.66 GHz Celeron personal computer, which was of the same order of the EMA method but at least 10 times faster than the RCWA-based method. This observation demonstrates that the CEMA method is not only accurate enough but also fast in calculation as compared with the RCWA-based method; hence it is especially suitable for the MBIR metrology.

B. Simulation of the Combined Extraction Method

To demonstrate the accuracy of the proposed extraction method combining ANN and LM algorithms, we performed simulations on the 1-D deep trench structure shown in Fig. 10(a), which is a typical two-layer structure consisting of a SiN layer and a Si layer above the silicon substrate. Figure 10(b) shows the effective optical model of the structure, in which the effective refractive index of each effective layer is calculated by the 1-D CEMA method.

An MLP type ANN with three layers was constructed. The input layer was chosen to contain 37 neurons that corresponded to 37 values of reflectivity in the wavelength range of 2 to 20 μm with an increment of 0.5 μm. The output of the ANN contained three neurons corresponding to the three trench parameters: trench width, depth of SiN layer, and depth of Si layer. A data set containing about 1000 pairs of trench parameters and reflectance spectrum were used to train the ANN. The trench parameters of the 1-D trench structure were generated randomly in the following range: trench width 80 to 120 nm, depth of SiN layer 120 to 180 nm, and depth of Si layer 3 to 7 μm. The pitches of the two layers are the same and fixed to 200 nm. The corresponding reflectance spectra were calculated with the CEMA modeling method. It took several hours to generate the training data set and then to perform the training on the 2.66 GHz Celeron personal computer.

Another data set containing 100 pairs of trench parameters and reflectance spectrum were used as samples to test the performance of the ANN and LM combined method. The trench parameters were generated randomly in the same range as for the training data set, but in this case the corresponding reflectance spectra were exactly calculated with the RCWA method and used as the "measured reflectance spectra." As expected, the trained ANN first generated a vector of geometric parameters from each of the "measured reflectance spectra" in a few milliseconds, with which as an initial estimate the LM algorithm then converged to a final solution with a few iterations in less than 2 s. As an example, Figure 11 depicts the errors and relative errors of the extracted depths in the Si layer for the 100 test samples. It is observed that all the extracted parameters are within a relative error of less than 0.2%. These excellent results demonstrate that the ANN/LM combined algorithm is sufficiently robust to solve the inverse spectral problem in MBIR metrology.

It is interesting to note that the ANN/LM combined extraction method always provides more accurate results than the ANN method alone. Table 1 presents one example of the results, in which the input trench parameters for simulation are trench width 105 nm, depth of SiN layer 152 nm, and depth of Si layer 4.3 μm. Figure 12 shows the reflectance spectra calculated from the above input parameters, from parameters extracted by the trained ANN alone, and from parameters extracted by the ANN/LM method. This observation verifies that the trained ANN alone can generate only a rough estimate of the parameters, which however as an initialization can guarantee the LM algorithm to rapidly converge to an accurate and global solution. The simulations thus demon-

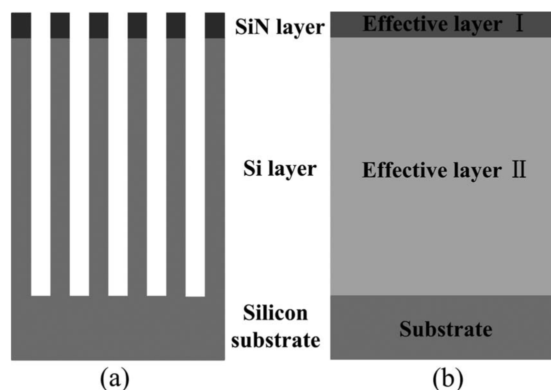

Fig. 10. (a) Structure of a 1-D deep trench with a SiN layer and a Si layer above the silicon substrate and (b) its effective optical model.

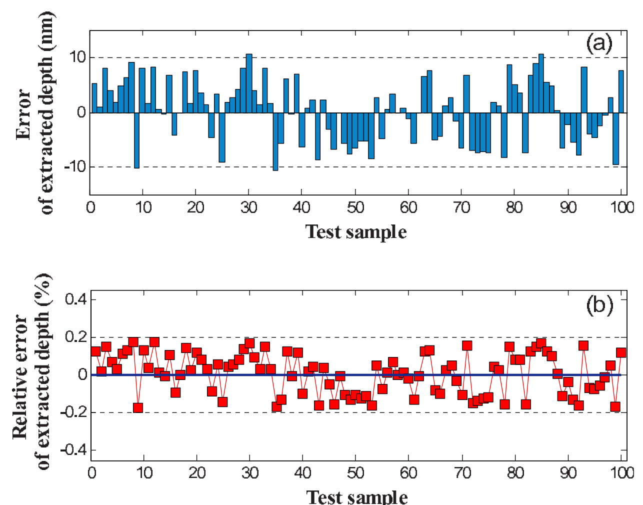

Fig. 11. (Color online) (a) Errors and (b) relative errors of extracted depths in Si layer for the 100 test samples.

Table 1. Parameters of the 1-D Trench Structure Extracted by ANN Alone and by ANN/LM Combined Method[a]

Trench Parameters	Trench Width		Depth of SiN Layer		Depth of Si Layer	
	Error (nm)	Relative Error	Error (nm)	Relative Error	Error (nm)	Relative Error
ANN	1.3	1.25%	4.1	2.71%	82	1.9%
ANN/LM	0.1	0.1%	0.2	0.13%	3	0.07%

[a]The input trench parameters for simulation: trench width 105 nm, depth of SiN layer 152 nm, depth of Si layer 4.3 μm.

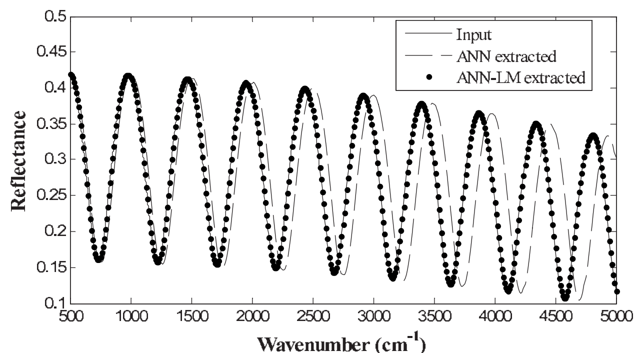

Fig. 12. Reflectance spectra calculated from the input parameters shown in Table 1, from parameters extracted by ANN alone and by ANN/LM method.

strate that the ANN/LM combined extraction method achieves improved performance over the ANN or LM method alone and leads to highly accurate measurement results as well as fast computation speed.

4. EXPERIMENTS

In order to obtain reflectance spectral signals to validate the improved MBIR metrology using the proposed CEMA modeling and the ANN/LM algorithm, an experimental platform was set up [24]. As shown in Fig. 13, the platform mainly consists of three parts, namely, an FTIR (Fourier transform infrared) spectrometer, a detection system, and a personal computer. An MIR 8025 FT Spectrometer from Newport was chosen as the FTIR spectrometer, which includes an IR source, a scanner, and an IR detector. The midinfrared light from the IR source is shaped into a small spot and projected onto the wafer

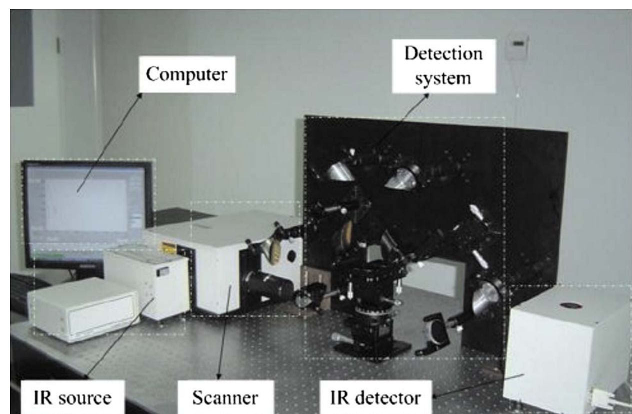

Fig. 13. (Color online) Experimental platform of the improved model-based infrared reflectrometry.

with trench structures at an incidence angle of 45° by the detection system, which was specially designed to be able to suppress reflections from the wafer backside and thus to eliminate spurious signal contributions. The reflectance signals are detected by the IR detector and converted into spectral signals, which are transported to the personal computer via a USB (universal serial bus) connection. Using a high-sensitivity MCT (mercury cadmium telluride) IR detector, the FTIR spectrometer-based platform can obtain spectral signals in a wide wavelength range of 0.7 to 28 μm with a very high accuracy.

A bottle trench structure with square lattice of cylindrical trenches of high aspect ratio was used as the specimen to test the performance of the improved MBIR metrology. Etched on silicon substrate and filled with poly silicon as electrodes, this bottle trench structure is a typical design in DRAM capacitors characterized by four geometric parameters: width of neck layer d_1, depth of neck layer h_1, width of bottle layer d_2, and depth of bottle layer h_2, as shown in Fig. 14(a). We modeled the structure as a two-layer stack and calculated the effective refractive index of each effective layer with the 2-D CEMA method as shown in Fig. 14(b).

To extract parameters of the bottle trench structure, we utilized the smooth part of the measured reflectance spectral signals in the wavenumber range of 1000 to 5000 cm^{-1}, which corresponds to the wavelength range of 10 to 2 μm. An MLP-type ANN was constructed with four neurons in the output layer and 17 neurons in the input layer, which respectively correspond to the four trench parameters and the 17 values of reflectance spectrum in the wavelength range of 2 to 10 μm with an increment of 0.5 μm. The ANN was trained with a data set containing pairs of trench parameters and reflectance spectrum. The trench parameters were generated by a combination of values randomly selected in the following ranges: d_1 100 to 140 nm, h_1 200 to 600 nm, d_2 160 to 200 nm, and h_2 3 to 6 μm. The reflectance spectra were calculated from the trench parameters generated by the CEMA modeling method.

After training the ANN, we extracted the trench parameters from the measured reflectance spectral signals using the proposed ANN/LM algorithm. The total time cost for each extraction of the four geometric parameters was < 2 s on the 2.66 GHz Celeron personal computer. Figure 15 depicts the fitted reflectance spectrum calculated from the extracted parameters compared with the reflectance spectrum measured by the experimental platform.

To further verify the accuracy of the improved MBIR metrology, the bottle trench structure was finally destruc-

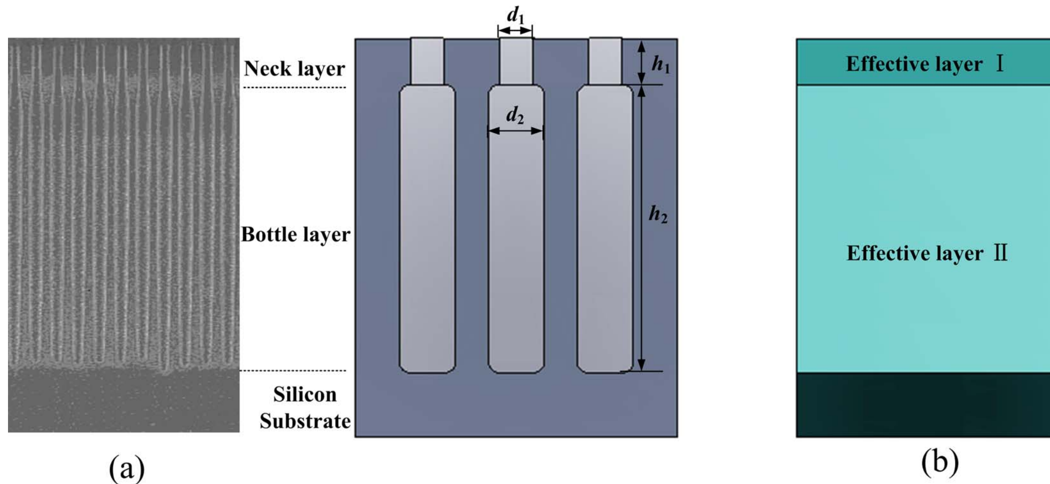

Fig. 14. (Color online) (a) SEM micrograph of the bottle trench structure and (b) its effective optical model.

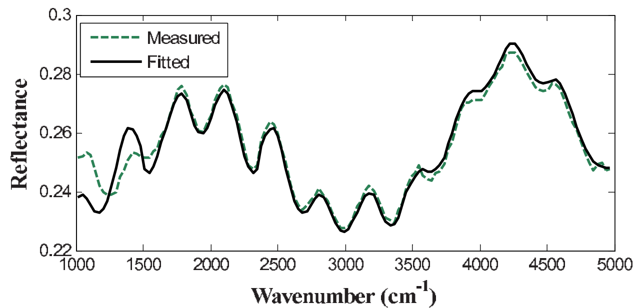

Fig. 15. (Color online) Fitted reflectance spectra calculated from the extracted parameters compared with the measured reflectance spectrum of the bottle trench structure.

tively measured with a cross-sectional SEM. In comparison with SEM, the improved MBIR metrology achieves an acceptable overall result as shown in Table 2. However, it is noted that the measured parameters of the neck layer are less accurate than those of the bottle layer. This may be due to the approximation accuracy of the 2-D CEMA modeling method, which seems to be more suitable for deeper trench layers. Further investigation will be conducted on the 2-D CEMA modeling method, especially on its independence of trench parameters such as trench depth and optical parameters such as incidence angle and polarization angle.

5. CONCLUSIONS

The success of MBIR metrology for measuring high-aspect-ratio deep trench structures relies heavily on accurate modeling of the trench structures and fast extraction of the trench parameters. In this paper, a modeling method called CEMA for accurate and fast reflectivity calculation of deep trench structures has been proposed. A method combining ANN and LM for robust and fast extraction of geometric parameters from the measured reflectance spectrum has also been developed.

The proposed CEMA method is based on the zeroth-order EMA, but a dispersion-corrected term is added to calculate the refractive index of each effective medium. The corrected term is solved analytically for 1-D trench structures but determined by a fitting-based approach for 2-D periodic trench array. Extensive simulations verify that the CEMA method is not only fast in calculation but also accurate enough in comparison with the RCWA method for both 1-D and 2-D trench structures, hence is especially suitable for the MBIR metrology.

In the process of parameter extraction with the ANN/LM combined method, an initial estimate of the trench parameters is quickly generated from the measured reflectance spectrum by the ANN, and then the accurate result is obtained by the LM algorithm. The trained ANN alone can only generate a rough estimate of the parameters, which however as an initialization can guarantee the LM algorithm to rapidly converge to an accurate and global solution. The combined extraction method is thus demonstrated to achieve improved performance over the ANN or LM method alone and leads to highly accurate measurement results as well as fast computation speed.

In contrast with traditional techniques such as SEM and AFM, the MBIR metrology is noncontact, nondestructive, time effective, and of low cost. Capable of operating in an ambient environment, this optical technique is especially suited to integrated metrology applications. It is expected that the improved MBIR metrology with accu-

Table 2. Parameters of the Bottle Deep Trench Measured by SEM and the Improved MBIR

Trench Parameter	Depth of Neck Layer (μm)	Width of Neck Layer (nm)	Depth of Bottle Layer (μm)	Width of Bottle Layer (nm)
SEM	0.411	123.4	4.513	185.7
MBIR	0.395	121.1	4.527	183.4
Relative error	3.9%	1.9%	0.31%	1.2%

rate modeling and fast extraction methods will provide an ideal tool for the measurement of within-wafer uniformity and wafer-to-wafer process variations, and thus has potential applications in on-line monitoring and process control for the fabrication of deep trench structures in DRAMs and power devices such as FinFETs at future technique nodes.

ACKNOWLEDGMENTS

The authors acknowledge financial support from the Hi-Tech Research and Development Program of China (grant 2006AA04Z325), National Natural Science Foundation of China (NSFC) (grant 50775090), National Basic Research Program of China (grant 2009CB724204), and Program for New Century Excellent Talent in Universitys of China (grant NCET-06-0639).

REFERENCES

1. U. Schroeder, S. Jakschik, A. Avellan, E. Erben, B. Hintze, R. Duschl, M. Kerber, A. Link, and A. Kersch, "Recent developments in ALD technology for 50 nm trench DRAM applications," ECS Trans. **1**, 125–132 (2006).
2. U. Rudolph, E. Weikmann, A. Kinne, A. Henke, P. VanHolt, S. Wege, A. Khan, S. Pamarthy, F. Schaftlein, and T. U. Lill, "Extending the capabilities of DRAM high aspect ratio trench etching," in *Proceedings of IEEE Conference on Advanced Semiconductor Manufacturing* (IEEE, 2004), pp. 89–92.
3. R. Srivastava, P. Yelehanka, H. A. Kek, S. L. Ng, V. Srinivasan, and R. Peltinov, "A novel approach to characterize trench depth and profile using the 3D tilt capability of a critical dimension-scanning electron microscope at 65 nm technology node," Proc. SPIE **6152**, 61524I (2006).
4. M. Watanabe, S. Baba, T. Nakata, T. Kurenuma, H. Kuroda, and T. Hiroki, "An advanced AFM sensor for high-aspect ratio pattern profile in-line measurement," Proc. SPIE **6152**, 61522A (2006).
5. E. Buhr, W. Michaelis, A. Diener, and W. Mirande, "Multi-wavelength VIS/UV optical diffractometer for high-accuracy calibration of nano-scale pitch standards," Meas. Sci. Technol. **18**, 667–674 (2007).
6. C. J. Raymond, M. Littau, R. Markle, and M. Purdy, "Scatterometry for shallow trench isolation (STI) process metrology," Proc. SPIE **4344**, 716–725 (2001).
7. A. A. Maznev, A. Mazurenko, C. A. Durán, and M. Gostein, "Measuring trench structures for microelectronics with model-based infrared reflectometry," AIP Conf. Proc. **931**, 74–78 (2007).
8. P. A. Rosenthal, C. A. Durán, J. Tower, and A. Mazurenko, "Model-based infrared metrology for advanced technology nodes and 300 mm wafer processing," AIP Conf. Proc. **788**, 620–624 (2005).
9. C. A. Durán, A. A. Maznev, G. T. Merklin, A. Mazurenko, and M. Gostein, "Infrared reflectometry for metrology of trenches in power devices," in *Proceedings of IEEE Conference on Advanced Semiconductor Manufacturing* (IEEE, 2007), pp. 175–179.
10. K. Chadan, D. Colton, L. Päivärinta, and W. Rundell, *An Introduction to Inverse Scattering and Inverse Spectral Problems* (SIAM, 1987).
11. X. Niu, N. Jakatdar, J. Bao, and C. J. Spanos, "Specular spectroscopic scatterometry," IEEE Trans. Semicond. Manuf. **14**, 97–111 (2001).
12. R. T. Zheng, N. Q. Ngo, L. N. Binh, and S. C. Tjin, "Two-stage hybrid optimization of fiber Bragg gratings for design of linear phase filters," J. Opt. Soc. Am. A **21**, 2399–2405 (2004).
13. K. Hehl, J. Bischoff, U. Mohaupt, M. Palme, B. Schnabel, L. Wenke, R. Bödefeld, W. Theobald, E. Welsch, R. Sauerbrey, and H. Heyer, "High-efficiency dielectric reflection gratings: design, fabrication, and analysis," Appl. Opt. **38**, 6257–6271 (1999).
14. R. P. Lippmann, "An introduction to computing with neural nets," IEEE ASSP Mag. **4**, 4–22 (1987).
15. I. Gereige, S. Robert, S. Thiria, F. Badran, G. Granet, and J. J. Rousseau, "Recognition of diffraction-grating profile using a neural network classifier in optical scatterometry," J. Opt. Soc. Am. A **25**, 1661–1667 (2008).
16. B. Kaplan, T. Novikova, A. D. Martino, and B. Drévillon, "Characterization of bidimensional gratings by spectroscopic ellipsometry and angle-resolved Mueller polarimetry," Appl. Opt. **43**, 1233–1240 (2004).
17. G. E. Jellison, "Physics of optical metrology of silicon-based semiconductor devices," in *Handbook of Silicon Semiconductor Metrology*, A. C. Diebold, ed. (Marcel Dekker, 2001), pp. 723–760.
18. S. M. Rytov, "Electromagnetic properties of a finely stratified medium," Sov. Phys. JETP **2**, 466–475 (1956).
19. S. Y. Liu, H. Y. Gu, C. W. Zhang, and H. W. Shen, "A fast algorithm for reflectivity calculation of micro/nano deep trench structures by corrected effective medium approximation," Acta Phys. Sin. **57**, 5996–6001 (2008).
20. W. H. Southwell, "Pyramid-array surface-relief structures producing antireflection index matching on optical surfaces," J. Opt. Soc. Am. A **8**, 549–553 (1991).
21. R. Bräuer and O. Bryngdahl, "Design of antireflection gratings with approximate and rigorous methods," Appl. Opt. **33**, 7875–7882 (1994).
22. P. Lalanne and D. L. Lalanne, "On the effective medium theory of subwavelength periodic structure," J. Mod. Opt. **43**, 2063–2085 (1996).
23. P. Lalanne and D. L. Lalanne, "Depth dependence of the effective properties of subwavelength gratings," J. Opt. Soc. Am. A **14**, 450–458 (1997).
24. S. Y. Liu, C. W. Zhang, H. W. Shen, and H. Y. Gu, "Model-based FTIR reflectometry measurement system for deep trench structures of DRAM," Spectrosc. Spectr. Anal. **29**, 935–939 (2009).